Journal of Organometallic Chemistry 694 (2009) 446–454

Contents lists available at ScienceDirect

Journal of Organometallic Chemistry

journal homepage: www.elsevier.com/locate/jorganchem

Mono- and dinuclear Pd(II) complexes of different salicylaldimine ligands as catalysts of transfer hydrogenation of nitrobenzene with cyclohexene and Suzuki–Miyaura coupling reactions

E. Tas [a,*], A. Kilic [a], M. Durgun [a], I. Yilmaz [b], I. Ozdemir [c], N. Gurbuz [c]

[a] Department of Chemistry, University of Harran, 63190 Sanliurfa, Turkey
[b] Department of Chemistry, Technical University of Istanbul, 34469 Istanbul, Turkey
[c] Department of Chemistry, Inonu University, 44280 Malatya, Turkey

ARTICLE INFO

Article history:
Received 11 September 2008
Received in revised form 7 November 2008
Accepted 7 November 2008
Available online 17 November 2008

Keywords:
Synthesis
Mono- and dinuclear Pd(II) complexes
Hydrogenation
Suzuki coupling reactions
Electrochemistry
Spectroelectrochemistry

ABSTRACT

In this study, the synthesis, spectroscopic, catalytic, and electrochemical properties of salicylaldimine Schiff-base ligands ($\mathbf{L_n}$) and their dinuclear Pd(II) complexes for $\mathbf{L_1}$ and $\mathbf{L_2}$ ligands with mononuclear Pd(II) complexes for $\mathbf{L_3}$ and $\mathbf{L_4}$ ligands were investigated. The ligands and their mono- or dinuclear Pd(II) complexes were characterized by FT-IR, UV–Vis, ^{1}H NMR and elemental analysis, as well as through magnetic susceptibility and spectroelectrochemical techniques. The catalytic studies showed that the introduction of *tert butyl* groups on the salicyl ring of the molecules increased the catalytic activity towards hydrogenation of nitrobenzene and cyclohexene in DMF at 25 and 45 °C. It was also observed that the steric hindered mono- and dinuclear Pd(II) complexes were thermally stable complexes and were not sensitive to air or the moisture. The complexes were easily prepared from cheap materials that could be used as versatile and efficient catalysts for different C–C coupling reactions (Suzuki–Miyaura reactions).

1. Introduction

The design, synthesis and characterization of salicylaldimine complexes are the subject of current interest due to their interesting structural, magnetic, spectral, catalytic and redox properties and are used as models for enzymes and various theoretical interests [1–8]. It is known that highly efficient catalytic systems are frequently used for selective transformations [9–12]. However, the design of efficient catalysts for large-scale applications is still a challenging problem. Noteworthy, a prerequisite for achieving high activity and selectivity is the fine tuning of the metal by introduction of ligands. Heterocyclic ligands containing nitrogen atoms are drawing a great deal of attention in coordination chemistry and homogeneous catalysis [2,13,14] because of the versatility of their steric and electronic properties which can be modified by choosing appropriate ring substituents [15,16]. As a catalyst, palladium is very important in pharmaceutical industry. However, it is expensive and toxic for large-scale applications. It is particularly important to reduce both its loss and presence in a product solution. The ability of transition metal catalysts to add or remove hydrogen from organic substrates by either direct or transfer hydrogenation process is a valuable synthesis tool [17]. Transition metal-catalyzed coupling reactions are one of the most important processes in organic chemistry and have been extensively studied since they represent a powerful and popular method for the formation of carbon–carbon bonds. This strategy has been applied to the synthesis of many organic compounds, especially the complex natural products, in supramolecular chemistry and in materials science [18–20]. The importance of biaryl units [19] as components of many kinds of compounds, mainly pharmaceuticals, herbicides and natural products, as well as in the field of engineering materials, such as conducting polymers, molecular wires and liquid crystals, has been attracted enormous interest from the chemistry community. Palladium and nickel-catalyzed Suzuki–Miyaura cross-coupling [21–23] is the most important and efficient strategy for the construction of unsymmetrical biaryl compounds. This cross-coupling methodology allows the use of organic solvents and inorganic bases, tolerates many functional groups, is not affected by steric hindrance of the substrates, and is suitable for industrial processes [24].

In the present study, the synthesis, spectroscopic characterization as well as reactivity in the hydrogenation of nitrobenzene and cyclohexene of mono and dinuclear palladium(II) metal complexes with steric hindered salicylaldimine ligands derived from 3,5-Bu^t_2-salicylaldehyde and different diamines are reported. The purpose of our study was to find a suitable, robust and easily prepared catalyst valid in a wide range of carbon–carbon

* Corresponding author.
E-mail address: etas@harran.edu.tr (E. Tas).

0022-328X/$ - see front matter © 2008 Elsevier B.V. All rights reserved.
doi:10.1016/j.jorganchem.2008.11.021

bond-forming processes. Therefore, the initial step was the selection of a potential catalytic system amenable to systematic structural and electronic variation. The fact that the steric hindered Pd(II) metal complexes are thermally stable and not sensitive to oxygen or moisture, as well as their ready economical synthetic access, prompted us to study their activity as catalysts in C–C bond-forming reactions. The other aim of this study is to establish a comparative electro-spectrochemical study on the new mono-and dinuclear Pd(II) complexes based on the different molecular structures with NONO donor sites.

2. Experimental

All reagents and solvents used in this study were of reagent-grade quality and obtained from commercial suppliers (Fluka, Merck and Aldrich). The elemental analyses were carried out in the facilities of Inonu University (Malatya, Turkey). The IR spectra were recorded on a Perkin Elmer Spectrum RXI FT-IR Spectrometer as KBr pellets. The ^{1}H and ^{13}C NMR spectra were recorded on a Bruker-Avence 300 MHz spectrometers. The Magnetic Susceptibilities were determined on a Sherwood Scientific Magnetic Susceptibility Balance (Model MK1) at room temperature (20 °C) using $Hg[Co(SCN)_4]$ as a calibrant; the diamagnetic corrections were calculated from Pascal's constants [25]. The electronic spectral studies were conducted on a Perkin Elmer model Lambda 25 UV–visible spectrophotometer in the wavelength 200–1100 nm. The cyclic voltammograms (CV) were carried out using CV measurements with Princeton Applied Research Model 2263 potentiostat controlled by an external PC. A three electrode system (BAS model solid cell stand) was used for CV measurements in DMSO and consisted of a 1.6 mm diameter of platinum disc electrode as working electrode, a platinum wire counter electrode, and an Ag/AgCl reference electrode. Tetra-*n*-butylammonium perchlorate (TBAP) was used as a supporting electrolyte. The reference electrode was separated from the bulk solution by a fritted-glass bridge filled with the solvent/supporting electrolyte mixture. The ferrocene/ferrocenium couple (Fc/Fc^+) was used as an internal standard but all the potentials in the paper were referenced to the Ag/AgCl reference electrode. The solutions containing ligands and mono- and dinuclear Pd(II) metal complexes were deoxygenated by a stream of high purity nitrogen for at least 5 min. before running the experiment and the solution was protected from air by a blanket of nitrogen during the experiment. The UV–Vis spectroelectrochemical experiments were performed with a home-built thin-layer cell which utilized a light transparent platinum gauze working electrode. A platinum wire counter electrode and a Ag/AgCl reference electrode were used for spectroelectrochemical cell. Potentials were applied and monitored with a Princeton Applied Research Model 2263 potentiostat. Time-resolved UV–Vis spectra were recorded on Agillent Model 8453 diode array spectrophotometer.

2.1. Synthesis of ligands

N,N′-[1,5-naphthalene]-3,5-Bu^t_2-salicylaldimine (**L₁**), *N,N′*-[2,7-fluarene]-3,5-Bu^t_2-salicylaldimine (**L₂**), *N,N′*-[1,8-naphthaline]-3,5-Bu^t_2-salicylaldimine (**L₃**) and *N,N′*-[3,4-benzophenon]-3,5-Bu^t_2-salicylaldimine) (**L₄**) ligands were synthesized by the reaction of 1.58 g (10 mmol) 1,5-diaminonaphthalene in 40 mL absolute methanol for (**L₁**), 1.96 g (10 mmol) 2,7-diaminofluarene in 40 mL absolute methanol for (**L₂**), 1.58 g (10 mmol) 1,8-diaminonaphthaline in 40 mL absolute methanol for (**L₃**) and 2.12 g (10 mmol) 3,4-diaminobenzofenonin in 40 mL absolute methanol for (**L₄**) and 4.70 g (20 mmol) 3,5-Bu^t_2-salicylaldehyde in 40 mL absolute methanol. Also, 3–4 drops of formic acid were added as catalyst. The mixtures were refluxed 48 h for (**L₁**) with (**L₂**) and 6–8 h for (**L₃**) with (**L₄**), followed by cooling to room temperature. The crystals were filtered in vacuum. The products were the recrystallized in ethanol. The products were soluble in common solvents such as $CHCl_3$, CH_3CH_2OH and DMF and DMSO.

2.1.1. For (*L₁*) ligand

Color: Yellow; m.p: 283 °C; Yield (%): 72; Anal. Calc. for $C_{40}H_{50}N_2O_2$ (F.W: 590.4 g/mol): C, 81.31; H, 8.53; N, 4.74. Found: C, 8.52; H, 8.42; N, 5.16%. ^{1}H NMR (75 MHz, $CDCl_3$, Me_4Si, ppm): δ = 13.68 (s, 2H, –O*H*, D-exchangeable), δ = 8.73 (s, 2H, *H*C=N), δ = 8.22–8.19 (d, 2H, *J* = 9, Ar–C*H*), δ = 7.58–7.49 (m, 4H, Ar–C*H*), δ = 7.29–7.21 (m, 4H, Ar–C*H*), δ = 1.51 (s, 18H, C–CH_3); δ = 1.34 (s, 18H, C–CH_3), ^{13}C NMR (300 MHz, $CDCl_3$, Me_4Si, ppm): 164.97 (*C*=N); 158.37, 146.50, 140.79, 137.10, 128.91, 127.01, 122.08, 118.63, 114.89 (Ar–*C*); 35.20, 34.25, 31.50, 29.47 (C–CH_3), IR (KBr pellets, ν_{max}/cm^{-1}): 1613 υ(C=N), 2865–2957 υ(Aliph C–H), 2480–3615 ν(OH···N). UV–Vis (λ_{max}, nm) in CH_2Cl_2: 241, 275, 375 and in DMSO: 275, 370.

2.1.2. For (*L₂*) ligand

Color: Yellow; m.p: 268 °C; Yield (%): 70; Anal. Calc. for $C_{43}H_{52}N_2O_2$ (F.W: 628.9 g/mol): C, 82.12; H, 8.33; N, 4.45. Found: C, 81.75; H, 8.25; N, 4.60%. ^{1}H NMR (75 MHz, $CDCl_3$, Me_4Si, ppm): δ = 13.84 (s, 2H, –O*H*, D-exchangeable), δ = 8.74 (s, 2H, *H*C=N), δ = 7.81–7.78 (d, 2H, *J* = 9, Ar–C*H*), δ = 7.51 (s, 2H, Ar–C*H*), δ = 7.47–7.46 (d, 4H, *J* = 3, Ar–C*H*), δ = 7.26–7.25 (d, 2H, *J* = 3, Ar–C*H*), δ = 3.98 (s, 2H, Cyc-CH_2), δ = 1.49 (s, 18H, C–CH_3); δ = 1.34 (s, 18H, C–CH_3), ^{13}C NMR (75 MHz, $CDCl_3$, Me_4Si, ppm): 162.90, 158,31 (*C*=N), 147,44, 144,77, 140,58, 139,93, 136,98, 127,96, 126,77, 120,59, 120,49, 118,43, 117,82 (Ar–*C*), 35.14, 34.03, 31.51, 29.45 (C–CH_3), 36,98 (*C*–CH_3) IR (KBr pellets, ν_{max}/cm^{-1}): 1619 υ(C=N), 2868–2906 υ(Aliph C-H), 2480–3680 υ(OH···N). UV–Vis (λ_{max}, nm) in CH_2Cl_2: 241, 283, 382, 392 and in DMSO: 254, 377, 382, 401.

2.1.3. For (*L₃*) ligand

Color: Dark White; m.p: 238 °C; Yield (%): 65; Anal. Calc. for $C_{40}H_{50}N_2O_2$ (F.W: 590.4 g/mol): C, 81.31; H, 8.53; N, 4.74. Found: C, 79.72; H, 8.06; N, 4.46%. ^{1}H NMR (300 MHz, $CDCl_3$, Me_4Si, ppm): δ = 13.58 (s, 2H, –O*H*, D-exchangeable), δ = 8.69 (s, 2H, *H*C=N), δ = 7.39–6.58 (m, 10H, Ar–C*H*), δ = 1.45 (s, 18H, C–CH_3); δ = 1.31 (s, 18H, C–CH_3), ^{13}C NMR (75 MHz, $CDCl_3$, Me_4Si, ppm): 153.94 (*C*=N), 141.36, 141.15, 137.34, 134.75, 126.80, 125.54, 124.23, 121.69, 118.89, 114.05, 107.11 (Ar–*C*), 31.63, 29.68, (C–CH_3), 35.28, 34.06 (C–CH_3) IR (KBr pellets, ν_{max}/cm^{-1}): 1602 υ(C=N), 2866–2954 υ(Aliph C–H), 3314 and 3410 υ(OH). UV–Vis (λ_{max}, nm) in CH_2Cl_2: 232, 287, 329, 343 and in DMSO: 285, 332, 347.

2.1.4. For (*L₄*) ligand

Color: Yellow; m.p: 146 °C; Yield (%): 75; Anal. Calc. for $C_{43}H_{52}N_2O_3$ (F.W: 644.4 g/mol): C, 80.09; H, 8.13; N, 4.34. Found: C, 79.78; H, 8.04; N, 4.46%. ^{1}H NMR (300 MHz, $CDCl_3$, Me_4Si, ppm): δ = 13.36 (s, 1H, –O*H*, D-exchangeable), 13.32 (s, 1H, –O*H*, D-exchangeable), δ = 8.71 (s, 1H, *H*C=N), δ = 8.70 (s, 1H, *H*C=N), δ = 7.88–7.20 (m, 12H, Ar–C*H*), δ = 1.44–1.43 (d, 18H, *J* = 3, C–CH_3); δ = 1.33–1.31 (d, 18H, *J* = 6, C–CH_3), ^{13}C NMR (300 MHz, $CDCl_3$, Me_4Si, ppm): 189.91 (*C*=O); 160.3, 159.9, 153.2, 153.0 (*C*=N); 140.9–112.6 (Ar–*C*); 25.9, 23.8 ve 29.5, 28.5 (C–CH_3). IR (KBr pellets, ν_{max}/cm^{-1}): 1657 υ(C=O), 1615 υ(C=N), 2869–2965 υ(Aliph C-H), 2219–3505 υ(OH···N). UV–Vis (λ_{max}, nm) in CH_2Cl_2: 284, 301, 408 and in DMSO: 263, 339.

2.2. Synthesis of mono- and dinuclear Pd(II) metal complexes

0.59 g, 1.0 mmol ligand (**L₁**), 0.63 g, 1.0 mmol ligand (**L₂**), 0.59 g, 1.0 mmol ligand (**L₃**) or 0.64 g, 1.0 mmol ligand (**L₄**) were dissolved

in absolute ethanol (50 mL). A solution of 0.43 g, 2.0 mmol of the palladium salt [**Pd(Ac)$_2$**] for [**Pd$_2$(L$_1$)$_2$**](**Ac**)$_4$, [**Pd$_2$(L$_2$)$_2$**](**Ac**)$_4$, [**Pd(L$_3$)**] and [**Pd(L$_4$)**] in absolute ethanol (30 mL), was added dropwise under argon atmosphere with continuous stirring. The stirred mixtures were then heated to the reflux temperature for 8 h and were maintained at this temperature. Then, the mixture was evaporated in vacuum and left to cool to room temperature. The compounds were filtered after adding 10 mL chloroform. The products were washed with a small amount of ethanol and water. The products were recrystallized from ethanol. Then they were dried at 100 °C in vacuum.

2.2.1. For [**Pd$_2$(L$_1$)$_2$**](**Ac**)$_4$

Color: Dark Green; m.p: >300 °C; Yield (%): 70; Anal. Calc. for [$C_{88}H_{108}N_4O_{12}Pd_2$] (F.W: 1616.6 g/mol): C, 64.98; H, 6.69; N, 3.44. Found: C, 64.72; H, 6.45; N, 3.73%. ^{1}H NMR (300 MHz, DMSO, Me_4Si, ppm): δ = 11.71 (s, 4H, –O*H*, D-exchangeable), δ = 9.98 (s, 4H, *H*C=N), δ = 7.96–6.92 (m, 16H, Ar–C*H*), δ = 1.60–1.10 (m, 72H, C–CH_3). IR (KBr pellets, ν_{max}/cm^{-1}): 1613 ν(C=N), 1646 ν(COO), 2869–2956 ν(Aliph-CH), 3280–3629 ν(OH). UV–Vis (λ_{max}, nm, * = shoulder peak) in CH_2Cl_2: 236, 271, 375, 496* and in DMSO: 262, 342, 483*.

2.2.2. For [**Pd$_2$(L$_2$)$_2$**](**Ac**)$_4$

Color: Green; m.p: 255 °C; Yield (%): 68; Anal. Calc. for [$C_{94}H_{112}N_4O_{12}Pd_2$] (F.W: 1692.6 g/mol): C, 66.31; H, 6.63; N, 3.29. Found: C, 66.13; H, 6.48; N, 3.16%. ^{1}H NMR (300 MHz, DMSO, Me_4Si, ppm): δ = 14.08 (s, 4H, –O*H*, D-exchangeable), δ = 9.98 (s, 4H, *H*C=N), δ = 8.02–7.42 (m, 16H, Ar–C*H*), δ = 4.04 (s, 4H, Cyc-CH_2), δ = 1.45–1.30 (m, 72H, C–CH_3). IR (KBr pellets, ν_{max}/cm^{-1}): 1618 ν(C=N), 1645 ν(COO), 2867–2957 ν(Aliph-CH), 3102–3677 ν(OH). UV–Vis (λ_{max}, nm) in CH_2Cl_2: 234, 389 and in DMSO: 268, 395.

2.2.3. For [**Pd(L$_3$)**]

Color: Black; m.p: >300 °C; Yield (%): 60; Anal. Calc. for [$C_{40}H_{48}N_2O_2Pd$] (F.W: 695.2 g/mol): C, 69.10; H, 6.96; N, 4.03. Found: C, 69.44; H, 6.68; N, 4.12%. IR (KBr pellets, ν_{max}/cm^{-1}): 1612 ν(C=N), 2866–2956 ν(Aliph-CH). UV–Vis (λ_{max}, nm, * = shoulder peak) in CH_2Cl_2: 232, 302, 353*, 478, 667* and in DMSO: 261, 318, 481*.

2.2.4. For [**Pd(L$_4$)**]

Color: Red; m.p: 185 °C; Yield (%): 65; Anal. Calc. for [$C_{43}H_{50}N_2O_3Pd$] (F.W: 749.3 g/mol): C, 68.93; H, 6.73; N, 3.74. Found: C, 68.45; H, 6.64; N, 3.83%. ^{1}H NMR (300 MHz, DMSO, Me_4Si, ppm): δ = 9.34–9.31 (d, 1H, J = 9, *H*C=N), δ = 8.79 (s, 1H, *H*C=N), δ = 8.55–7.46 (m, 12H, Ar–C*H*), δ = 1.49 (s, 18H, C–CH_3), δ = 1.31–1.30 (d, 18H, J = 3, C–CH_3). ^{13}C NMR (300 MHz, DMSO, Me_4Si, ppm): 195.1 (*C*=O); (165.4, 164.8) and (156.3, 156.3) (*C*=N); 146.6, 143.8, 140.2, 139.8, 137.3, 136.6, 136.4, 136.3, 133.6, 131.7, 131.3, 130.4, 130.1, 129.2, 128.7, 120.9, 119.2 (Ar–*C*); 36.1, 34.2 and 29.9, 29.6 (C–CH_3). IR (KBr pellets, ν_{max}/cm^{-1}): 1655 ν(C=O), 1610 ν(C=N), 2850–2980 ν(Aliph-CH). UV–Vis (λ_{max}, nm) in CH_2Cl_2: 255, 333, 376, 412, 488 and in DMSO: 258, 330, 371, 482.

2.3. Hydrogenation procedure

The hydrogenation of nitrobenzene and cyclohexene was carried out in a thermostatic reaction flask (100 mL) at 25 and 45 °C under 760 Torr H_2 with vigorous stirring in dry and deoxygenated 50 mL DMF solution. A catalyst was added into 50 mL DMF and saturated with H_2 gas for 10–15 min. After addition of $NaBH_4$, the mixture was stirred for ca. 5 min and then nitrobenzene and cyclohexene were transferred into vessel. Then the H_2 gas was bubbled again into the flask and the volume of the absorbed H_2 gas was measured periodically. Nitrobenzene and Cyclohexene, as identified by means of IR scanning, were completely reduced to aniline and cyclohexane.

2.4. General procedure for the Suzuki–Miyaura coupling reaction

The catalyst (1.0 mmol% of Pd complexes), aryl halides (1.0 mmol), phenyl boronic acid (1.5 mmol), K_2CO_3 (2.0 mmol), diethyleneglycol-di-*n*-butylether as internal standart (30 mg), DMF (3 mL) were all added to a small Schlenk tube and the mixture was heated at 100 °C for 10 h in an oil bath. At the end, the mixture was cooled, filtered and concentrated. The purity of the compounds was checked by GC with NMR and the yields were based on different aryl halides.

3. Results and discussion

3.1. Synthesis and characterization

The reaction steps for the synthesis of the ligands and their mono- and dinuclear palladium(II) complexes are given in Schemes 1 and 2. In the first step, the ligands (**L$_1$**), (**L$_2$**) (**L$_3$**) and (**L$_4$**) were synthesized by the condensation of 3,5-Bu$^t_2$-salicylaldehyde with different diamines. In the second step, the mono- and dinuclear Pd(II) metal complexes were synthesized by the condensation of ligands with palladium acetate salt. For the structural characterization of ligands (**L$_1$**), (**L$_2$**) (**L$_3$**) and (**L$_4$**) with their mono- and dinuclear Pd(II) complexes elemental analyses, IR spectra, UV–Vis spectra, ^{1}H NMR spectra, and magnetic susceptibility measurements were used and the corresponding data are given in experimental section. The reactivity in the hydrogenation of nitrobenzene and cyclohexene of mono- and dinuclear Pd(II) complexes are reported. Also, the catalytic activity of mono- and dinuclear Pd(II) complexes were tested in the Suzuki–Miyaura coupling reaction. The mono- and diuclear Pd(II) metal complexes were catalysed Suzuki–Miyaura coupling reaction between phenylboronic acid and different arylbromides affording biphenyls. The metal to ligand ratios in the dinuclear Pd(II) complexes were found to be 2:2 for [**Pd$_2$**(L$_1$)$_2$](**Ac**)$_4$ and [**Pd$_2$**(L$_2$)$_2$](**Ac**)$_4$ and in the mononuclear Pd(II) complexes were found to be 1:1 for [**Pd(L$_3$)**] and [**Pd(L$_4$)**].

The ^{1}H and ^{13}C NMR spectral results obtained for (**L$_n$**) ligands and their mono- and dinuclear Pd(II) complexes in $CDCl_3$ and DMSO, with their assignments, are given in the experimental section. The proton resonance appearing as a broad low intensity singlet at δ = 13.84–13.32 ppm in the spectra (**L$_n$**) due to the OH/NH protons involved in intramolecular H-bonding. In contrast to expectation, in the ^{1}H NMR spectra of dinuclear Pd(II) complexes, a broad singlet peak in a low intensity appeared at δ = 14.08–11.71 ppm due to the presence of the OH protons involved in the dinuclear Pd(II) complexes. This result indicates that the (**L$_1$**) and (**L$_2$**) ligands are coordinated by the palladium center through the azomethine nitrogen and aromatic carbon [26]. These characteristic bands are not observed in the ^{1}H NMR spectra of mononuclear Pd(II) complexes, which indicates that the (**L$_3$**) and (**L$_4$**) ligands are coordinated by palladium center through the azomethine nitrogen and phenolic oxygen. All protons of azomethine and salicylic moieties of these complexes were shifted upfield while the aromatic ring protons exhibited either downfield shift or remained unchanged (in Section 2) compared with those of the free ligands. Similar magnetic shielding effects were previously observed in the Schiff-base complexes of Pd(II), Zn(II), Co(II) and Cu(II) [27–30]. In the ^{13}C NMR, the imine carbon resonance was found at 164.97 ppm for (**L$_1$**), 162.90 and 158.31 ppm for (**L$_2$**), 153.94 ppm for (**L$_3$**) and 160.30, 159.90, 153.20, 153.0 ppm for (**L$_4$**), respec-

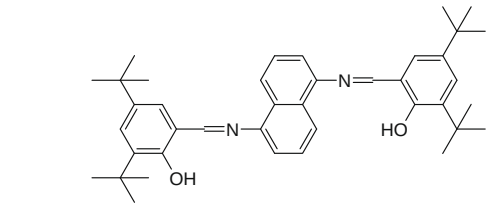

(L_1)

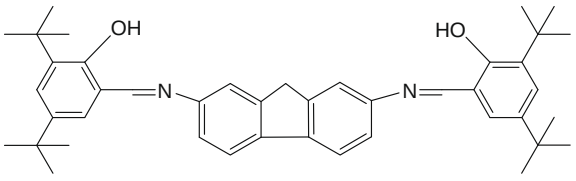

(L_2)

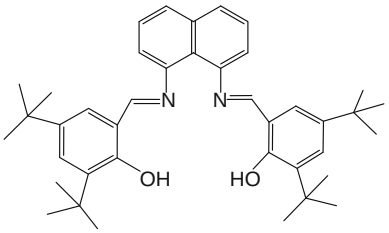

(L_3)

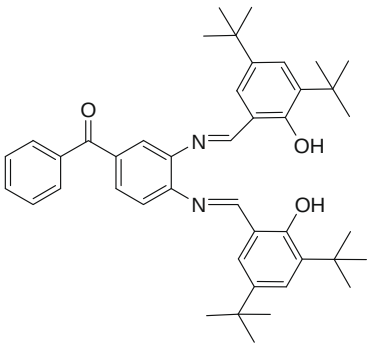

(L_4)

Scheme 1. Supposed structures of the ligands ($\mathbf{L_n}$).

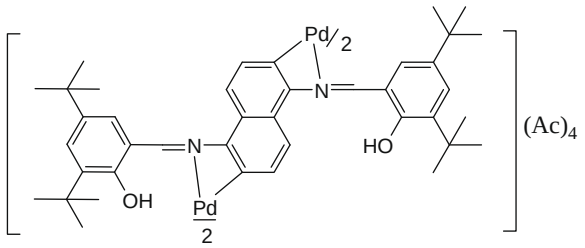

$[Pd_2(L_1)_2](Ac)_4$

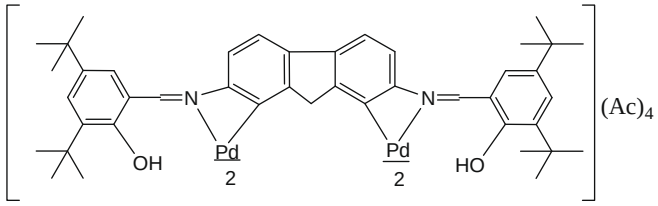

$[Pd_2(L_2)_2](Ac)_4$

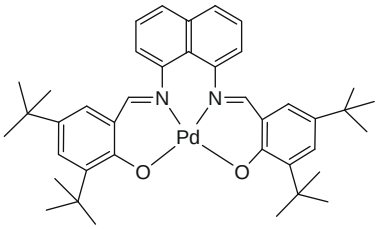

$[Pd(L_3)]$

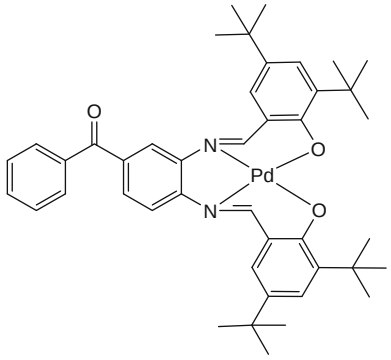

$[Pd(L_4)]$

Scheme 2. Supposed structures dinuclear and mono Pd(II) complexes.

tively. The carbonyl carbon resonance was found at 189.91 ppm for ($\mathbf{L_4}$) and shifted to higher frequency when compared with the mononuclear [**Pd($\mathbf{L_4}$)**] complex.

The main stretching frequencies of the IR spectra of ligands ($\mathbf{L_n}$) and their mono- and dinuclear Pd(II) complexes are given in the experimental section. The IR spectra of ligands and their corresponding Pd(II) complexes are found to be very similar to each other. Hence, significant frequencies are selected by comparing the IR spectra of the ligands with those of mono- and dinuclear Pd(II) complexes. The IR of ligands are characterized by the appearance of a band at between 2219 and 3680 cm^{-1} due to the ν(OH···N) or ν(OH)groups [31,32]. In the IR spectra of mononuclear [**Pd($\mathbf{L_3}$)**] and [**Pd($\mathbf{L_4}$)**] complexes, these bands disappeared. In contrast to expectation, in the IR spectra of dinuclear [**$Pd_2(L_1)_2$**]($\mathbf{Ac}$)$_4$ and [**$Pd_2(L_2)_2$**]($\mathbf{Ac}$)$_4$ complexes, these absorption bands did not disappear. These results indicate deprotonation of the phenolic proton of the ($\mathbf{L_3}$) and ($\mathbf{L_4}$) ligands and not deprotonation of the phenolic proton of the ($\mathbf{L_1}$) and ($\mathbf{L_2}$) ligands prior to coordination. The free ligands showed strong peaks at 1602–1619 cm^{-1}, which are characteristic of the azomethine ν(C=N) group [33]. In the case of the complexes, these bands were shifted to the lower or higher frequencies, indicating that the nitrogen atoms of the azomethine groups are coordinated to the palladium ion as expected [34]. In the IR spectra of the dinuclear Pd(II) complexes, a strong peak observed at 1646–1645 cm^{-1} was assigned to acetate ν(COO) stretching. This peak was not observed in the free ligands.

Electronic spectra of ligands and their mono- and dinuclear Pd(II) complexes were recorded in the 200–1100 nm range in CH_2Cl_2 and DMSO solutions, and the results are given in the experimental section. The electronic spectra of ligands and their Pd(II) metal complexes in CH_2Cl_2 and DMSO solutions showed absorption bands at 232–667 nm. In the electronic spectra of the ligands and their Pd(II) complexes, the wide range bands seem to be due to both the $\pi \rightarrow \pi^*$and $n \rightarrow \pi^*$ of C=N chromophore or charge-transfer

transition arising from π electron interactions between the metal and ligand which involves either a metal-to-ligand or ligand-to-metal electron transfer and d–d transitions [35,36]. The absorption bands observed within the range of 232–408 nm in CH_2Cl_2 or DMSO are most probably due to the transition of $\pi \rightarrow \pi^*$ transitions in the benzene ring or $n \rightarrow \pi^*$ of imine group corresponding to the ligands and their mono- and dinuclear Pd(II) metal complexes [37]. The electronic spectra of Pd(II) metal complexes in CH_2Cl_2 and DMSO solutions show absorption bands at between 481 and 496 nm are assigned to metal to ligand charge-transfer (MLCT) and $^1A_{1g} \rightarrow {}^1B_{1g}$ transitions, respectively, [38]. Surprisingly, the electronic spectrum of [Pd(L_3)] complex in CH_2Cl_2 is different from that of the other metal complexes. The absorbance at 667 nm in the spectra of [Pd(L_3)] probably originates from a $Pd(d\pi) \rightarrow \pi^*$ transition [30].

Magnetic susceptibility measurement provides sufficient data to characterize the structure of the metal complexes. Magnetic moment measurements of the compounds were carried out at 25 °C. The room temperature magnetic moments of Pd(II) metal complexes are observed diamagnetic properties. The Pd(II) metal complexes were diamagnetic, thus their ^1H NMR and ^{13}C NMR spectra could be obtained. With a view to studying the electrolytic nature of the metal complexes, their molar conductivities were measured in DMF at 10^{-3} M. The **[Pd$_2$(L_1)$_2$](Ac)$_4$** and **[Pd$_2$(L_2)$_2$](Ac)$_4$** metal complexes with counter acetate ions have high molar conductivity (Λ_M) values at room temperature, indicating their almost electrolytic nature. As expected, **[Pd(L_3)$_2$]** and **[Pd(L_4)$_2$]** metal complexes were very poor in molar conductivity which indicate that these metal complexes had no electrolytic nature.

3.2. Catalytic studies

3.2.1. Catalytic reduction of nitrobenzene and cyclohexene by Pd(II) complexes

The catalytic studies showed that the mono- and dinuclear metal complexes (except for **[Pd(L_3)]** complex at 45 °C) exhibited a catalytic activity toward the hydrogenation of nitrobenzene and cyclohexene under H_2 gas (760 Torr) in DMF solution at 25 and 45 °C (Schemes 3 and 4). Nitrobenzene and cyclohexene, as identified by means of IR scanning, were completely reduced to aniline and cyclohexane. Although addition of $NaBH_4$ to the catalysts solution prior to the introduction of H_2 accelerated their catalytic activity, the hydrogenation generally did not need any preliminary activation (Tables 1 and 2, Figs. 1–5) The conditions, initial rate absorption of H_2, and specific activity for four complexes are presented in Tables 1 and 2. The course of reduction for some mono- and dinuclear Pd(II) catalysts are shown in Figs. 1–5. The initial rate

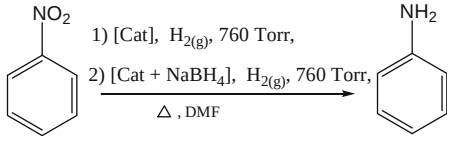

Scheme 3. Catalytic activity of Pd(II) complexes at 760 Torr of H_2 and 25 and 45 °C for nitrobenzene.

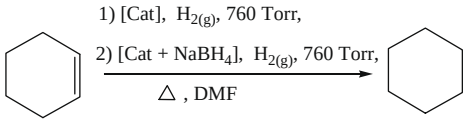

Scheme 4. Catalytic activity of Pd(II) complexes at 760 Torr of H_2 and 25 and 45 °C for cyclohexene.

Table 1
Conditions, initial rate of H_2 absorption, catalytic activity of Pd(II) complexes at 760 Torr of H_2 and 25 and 45 °C for nitrobenzene.

Compounds	[Cat] (10^{-5} mol/L)	C_{PhNO2} (10^{-2} mol/L)	Initial rate of H_2 W absorption (mmol/min)	Specific activity Mol H_2/mol-cat (min)
[Pd$_2$(L_1)$_2$](Ac)$_4$	10.0	1.46	0.04	0.72 (25 °C)
	8.6	1.46	0.03	0.54 (45 °C)
	7.9	1.27	0.01	0.11 (25 °C + $NaBH_4$)
[Pd$_2$(L_2)$_2$](Ac)$_4$	5.8	1.46	0.01	0.60 (25 °C)
	6.6	1.27	0.02	0.53 (45 °C)
	6.1	1.46	0.03	0.49 (25 °C + $NaBH_4$)
[Pd(L_3)]	11.5	1.01	0.00	0.30 (25 °C)
	19.3	1.27	-	0.00 (45 °C)
	15.8	1.44	0.09	1.22 (25 °C + $NaBH_4$)
[Pd(L_4)]	12.3	1.01	0.01	0.18 (25 °C)
	12.2	1.56	0.01	0.25 (25 °C + $NaBH_4$)

Table 2
Conditions, initial rate of H_2 absorption, catalytic activity of Pd(II) complexes at 760 Torr of H_2 and 25 and 45 °C for cyclohexene.

Compounds	[Cat] (10^{-5} mol/L)	C_{PhNO2} (10^{-2} mol/L)	Initial rate of H_2 W Absorption (mmol/min)	Specific activity Mol H_2/mol-cat (min)
[Pd$_2$(L_1)$_2$](Ac)$_4$	17.1	3.64	0.03	0.65 (25 °C)
	17.3	3.64	0.04	0.70 (45 °C)
	16.2	3.64	0.02	0.37 (25 °C + $NaBH_4$)
	16.9	3.64	0.02	0.45 (45 °C + $NaBH_4$)
[Pd$_2$(L_2)$_2$](Ac)$_4$	18.1	3.64	0.02	0.52 (25 °C)
	17.8	3.64	0.04	0.64 (45 °C)
	16.4	3.64	0.02	0.44 (25 °C + $NaBH_4$)
	14.3	3.64	0.03	0.40 (45 °C + $NaBH_4$)
[Pd(L_3)]	38.1	3.64	0.02	0.53 (25 °C)
	36.7	3.64	0.05	0.83 (45 °C)
	37.4	3.64	0.01	0.43 (25 °C + $NaBH_4$)
	40.3	3.64	0.02	0.41 (45 °C + $NaBH_4$)
[Pd(L_4)]	36.7	3.64	0.02	0.47 (25 °C)
	36.0	3.64	0.02	0.46 (45 °C)
	33.4	3.64	0.01	0.25 (25 °C + $NaBH_4$)
	40.0	3.64	0.01	0.32 (45 °C + $NaBH_4$)

of H_2 absorption and the specific catalytic activity approximately identical for all mono- and dinuclear Pd(II) metal complexes. The results indicate that introduction of Bu^t_2 groups on the salicylaldimine ring increases the catalytic activity of all complexes. The electron-donating Bu^t_2 and other functional groups probably increases the electron density on the Pd atom, which is subjected to electrophilic attack by a nitro group of nitrobenzene and double band of cyclohexene [30]. The specific catalytic activity of the mono- and dinuclear Pd(II) metal complexes decreases due to linked different ligands and functional groups.

3.2.2. Suzuki coupling reaction

Suzuki cross-coupling represents a powerful method for C–C bond formation [39]. Recently, the Suzuki reaction of aryl halides catalysed by palladium/tertiary phosphine [40] and palladium/

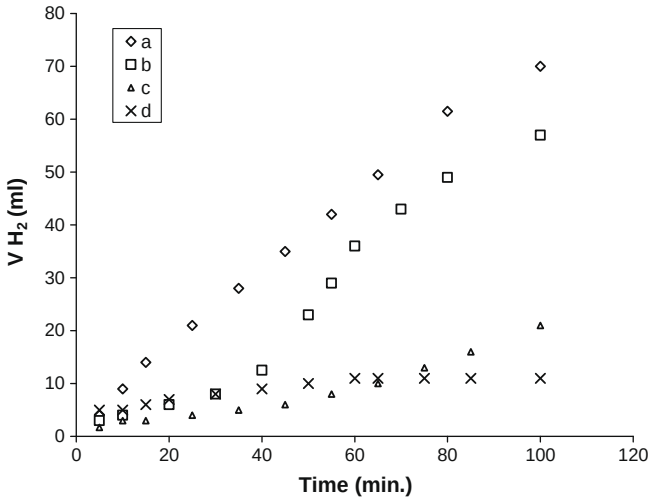

Fig. 1. Hydrogenation of nitrobenzene as catalysts Pd(II) complexes at 25 °C in DMF solution. (a = [**Pd$_2$(L$_1$)$_2$**](**Ac**)$_4$, b = [**Pd$_2$(L$_2$)$_2$**](**Ac**)$_4$, c = [**Pd(L$_3$)**] and d = [**Pd(L$_4$)**]).

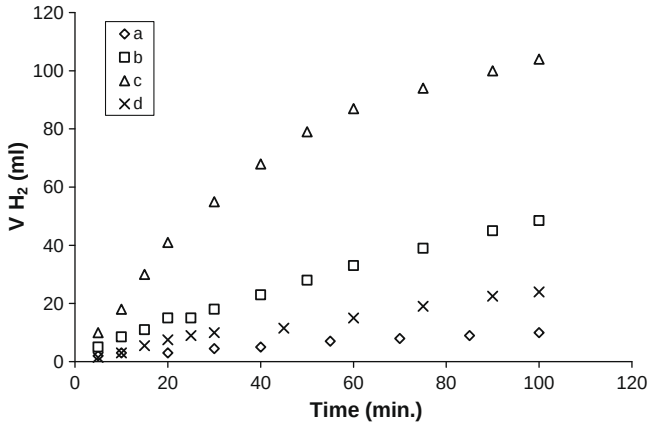

Fig. 2. Hydrogenation of nitrobenzene as catalysts Pd(II) complexes + $NaBH_4$ at 25 °C in DMF solution. (a = [**Pd$_2$(L$_1$)$_2$**](**Ac**)$_4$, b = [**Pd$_2$(L$_2$)$_2$**](**Ac**)$_4$, c = [**Pd(L$_3$)**] and d = [**Pd(L$_4$)**]).

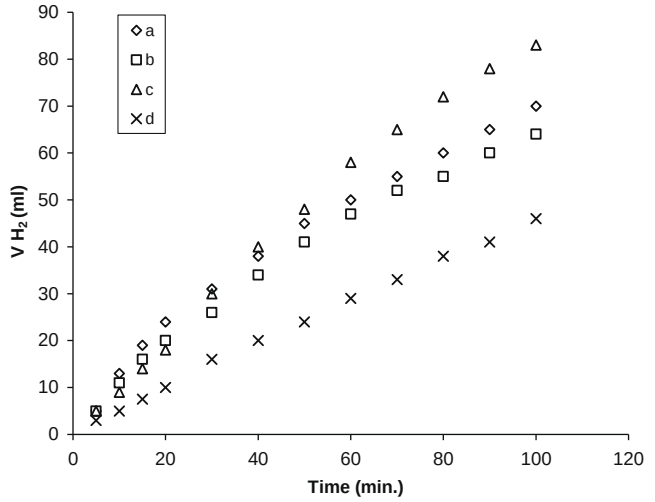

Fig. 3. Hydrogenation of cyclohexene as catalysts Pd(II) complexes at 45 °C in DMF solution. (a = [**Pd$_2$(L$_1$)$_2$**](**Ac**)$_4$, b = [**Pd$_2$(L$_2$)$_2$**](**Ac**)$_4$, c = [**Pd(L$_3$)**] and d = [**Pd(L$_4$)**]).

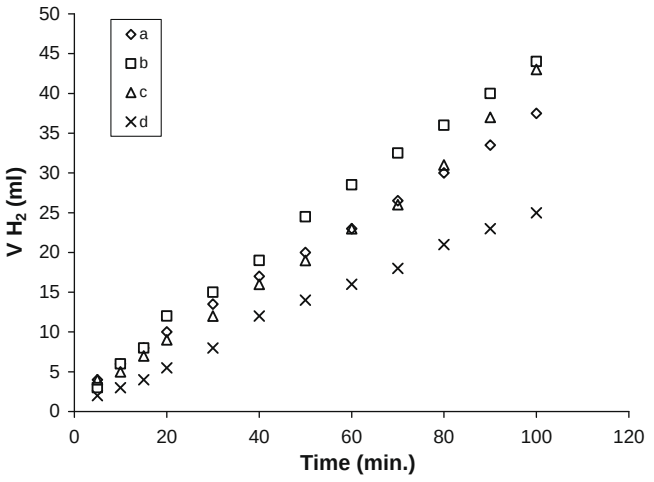

Fig. 4. Hydrogenation of cyclohexene as catalysts Pd(II) complexes + $NaBH_4$ at 25 °C in DMF solution. (a = [**Pd$_2$(L$_1$)$_2$**](Ac)$_4$, b = [**Pd$_2$(L$_2$)$_2$**](Ac)$_4$, c = [**Pd(L$_3$)**] and d = [**Pd(L$_4$)**]).

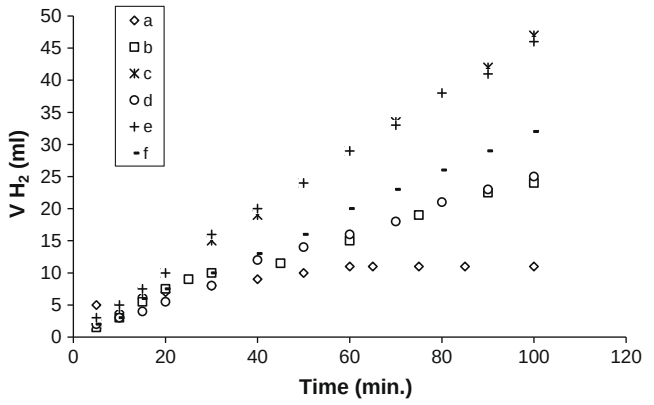

Fig. 5. Hydrogenation of nitrobenzene and cyclohexene as [**Pd(L$_4$)**] catalysts at 25 and 45 °C in DMF solution. (a = nitrobenzene (25 °C), b = nitrobenzene + $NaBH_4$ (25 °C), c = cyclohexene (25 °C), d = cyclohexene + $NaBH_4$ (25 °C), e = cyclohexene (45 °C) and f = cyclohexene + $NaBH_4$ (45 °C).

NHC [41,42] systems have been extensively studied due to the economically attractive nature of the starting materials and the production of the less toxic salt by-products e.g. NaX (X: Cl, Br, and I). To survey the parameters for the Suzuki reaction, we chose to examine Cs_2CO_3, K_2CO_3, and K_3PO_4 as base and DMF, toluene and dioxane as the solvent. It was found that the reactions performed in DMF with Cs_2CO_3 or K_2CO_3 at 100 °C showed the best performance (Scheme 5). We started our investigation with the coupling of 4-bromoacetophenone and phenylboronic acid, in the presence of [**Pd$_2$(L$_1$)$_2$**](**Ac**)$_4$, [**Pd$_2$(L$_2$)$_2$**](**Ac**)$_4$, [**Pd(L$_3$)**] and [**Pd(L$_4$)**] metal complexes. Table 3 summarizes the results obtained in the presence of [**Pd$_2$(L$_1$)$_2$**](**Ac**)$_4$, [**Pd$_2$(L$_2$)$_2$**](**Ac**)$_4$, [**Pd(L$_3$)**] and [**Pd(L$_4$)**] metal complexes (Table 3 entries 1–4). It can be seen that the palladium complexes listed in Table 3 are effective compounds for the coupling of aryl bromides with phenylboronic acid (Table 3, entries 1–12).

3.3. Electrochemistry and spectroelectrochemistry

Electrochemistry of the ligands and their palladium complexes were studied by cyclic voltammetry in scan rate of 0.010 V s^{-1} in dichloromethane (CH_2Cl_2) solution containing 0.1 M TBAP support-

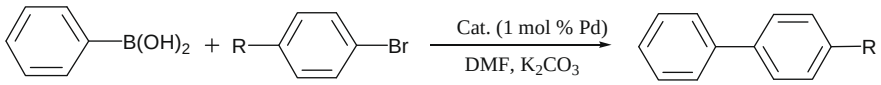

Scheme 5. The Suzuki–Miyaura coupling of different aryl halides with phenylboronic acid.

Table 3
The Suzuki–Miyaura coupling of different aryl halides with phenylboronic acid.

Entry	R	[Cat]	Yield[a,b,c,d] (%)
1	$COCH_3$	$[\mathbf{Pd_2(L_1)_2}]$ $(\mathbf{Ac})_4$	83
2	$COCH_3$	$[\mathbf{Pd_2(L_2)_2}]$ $(\mathbf{Ac})_4$	73
3	$COCH_3$	$[\mathbf{Pd(L_3)}]$	81
4	$COCH_3$	$[\mathbf{Pd(L_4)}]$	77
5	NO_2	$[\mathbf{Pd_2(L_1)_2}]$ $(\mathbf{Ac})_4$	95
6	NO_2	$[\mathbf{Pd_2(L_2)_2}]$ $(\mathbf{Ac})_4$	96
7	NO_2	$[\mathbf{Pd(L_3)}]$	86
8	NO_2	$[\mathbf{Pd(L_4)}]$	96
9	CHO	$[\mathbf{Pd_2(L_1)_2}]$ $(\mathbf{Ac})_4$	84
10	CHO	$[\mathbf{Pd_2(L_2)_2}]$ $(\mathbf{Ac})_4$	82
11	CHO	$[\mathbf{Pd(L_3)}]$	78
12	CHO	$[\mathbf{Pd(L_4)}]$	90

[a] Reaction conditions: 1.0 mmol of *p*-R-C_6H_4Br, 1.5 mmol phenylboronic acid, 2 mmol K_2CO_3, % 1.0 mol Pd, 3 mL DMF.
[b] Purity of all compounds determined by NMR and the yield calculated on the aryl bromide.
[c] All reactions followed by GC.
[d] Temperature 100 °C and time 10 h.

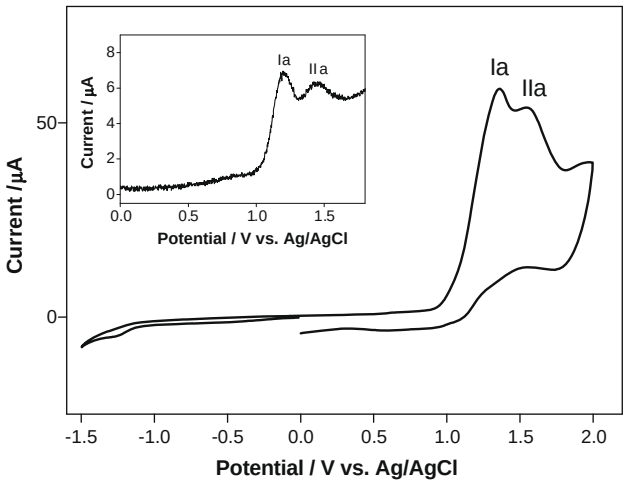

Fig. 7. Cyclic voltammogram (CV) of $[\mathbf{Pd_2(L_2)_2}](\mathbf{Ac})_4$, in CH_2Cl_2 containing 0.1 M TBAP. Scan rate: 0.010 V s^{-1}. Working electrode: a 1.6 mm diameter of platinum disc electrode. c = 4.0 × 10^{-3} M. The inset figure shows DPV of $[\mathbf{Pd_2(L_2)_2}](\mathbf{Ac})_4$ in the same experimental conditions.

ing electrolyte. Only $\mathbf{L_2}$ and $\mathbf{L_4}$ ligands and their palladium complexes exhibited well-defined voltammograms in the scale of 2.0 to −1.8 V. Cyclic voltammograms (CVs) of these ligands are given in Fig. 6. $\mathbf{L_2}$ and $\mathbf{L_4}$ ligands exhibited one oxidation wave (Ia) without corresponding cathodic wave indicating an irreversible process. The anodic peak potentials of $\mathbf{L_2}$ and $\mathbf{L_4}$ (E_{pa}) were located at 1.37 and 1.20 V versus Ag/AgCl in the scan rate of 0.010 V s^{-1}, respectively. $\mathbf{L_4}$ also displayed one irreversible reduction process at 1.45 V (E_{pc}). Fig. 7 shows the CV of $[\mathbf{Pd_2}(L_2)_2](\mathbf{Ac})_4$ where the inset figure presents differential pulse voltammogram (DPV) of the complex in the same experimental conditions. $[\mathbf{Pd_2}(L_2)_2](\mathbf{Ac})_4$ exhibited two anodic waves (Ia and IIa) without corresponding cathodic waves which were assigned to irreversible processes. The combined anodic waves (Ia and IIa) observed for the CV of $[\mathbf{Pd_2}(L_2)_2](\mathbf{Ac})_4$ could be clearly separated by the DPV (the inset figure). In view of the CV of $\mathbf{L_2}$, it can be concluded that the first and second oxidation processes are probably based on the ligand and palladium metal center, respectively. Fig. 8 represents the CV of $[\mathbf{Pd_2}(L_4)_2](\mathbf{Ac})_4$ where the inset figure introduces DPV of the palladium complex during anodic and cathodic scan. $[\mathbf{Pd_2}(L_4)_2](\mathbf{Ac})_4$ exhibited a single one electron reversible oxidation and a quasi-reversible reduction. The half-wave potentials of the oxidation and reduction processes were located at $E_{1/2}$ = 1.13 and −1.22 V versus Ag/AgCl in the scan rate of 0.010 V s^{-1}, respectively. The reduction and oxidation waves of $[\mathbf{Pd_2}(L_4)_2](\mathbf{Ac})_4$ appeared at almost the same position with those of $\mathbf{L_4}$ ligand, which indicates that the reduction and oxidation process of the complex are based

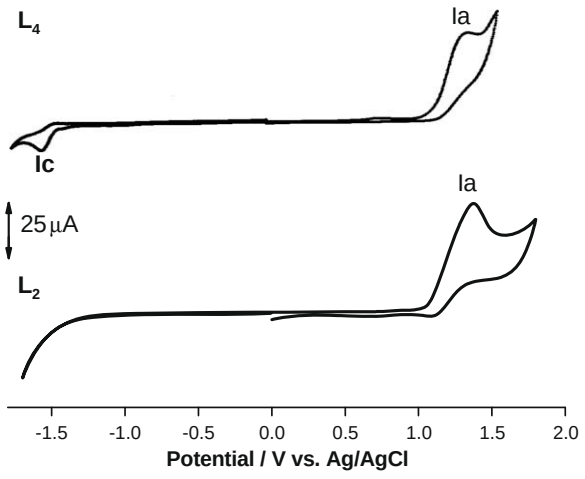

Fig. 6. Cyclic voltammograms (CVs) of $\mathbf{L_2}$ and $\mathbf{L_4}$ in CH_2Cl_2 containing 0.1 M TBAP. Scan rate: 0.010 V s^{-1}. Working electrode: a 1.6 mm diameter of platinum disc electrode. c = 4.0 × 10^{-3} M.

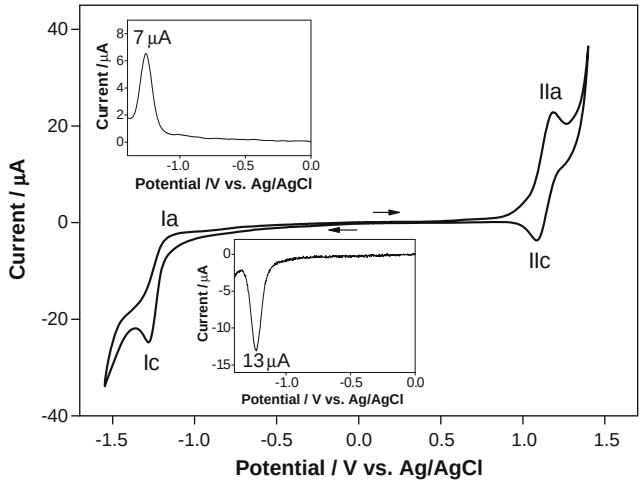

Fig. 8. Cyclic voltammogram (CV) of $[\mathbf{Pd_2(L_4)_2}](\mathbf{Ac})_4$ in CH_2Cl_2 containing 0.1 M TBAP. Scan rate: 0.010 V s^{-1}. Working electrode: a 1.6 mm diameter of platinum disc electrode. c = 4.0 × 10^{-3} M. The inset figures show DPV of $[\mathbf{Pd_2(L_4)_2}](\mathbf{Ac})_4$ in the same experimental conditions.

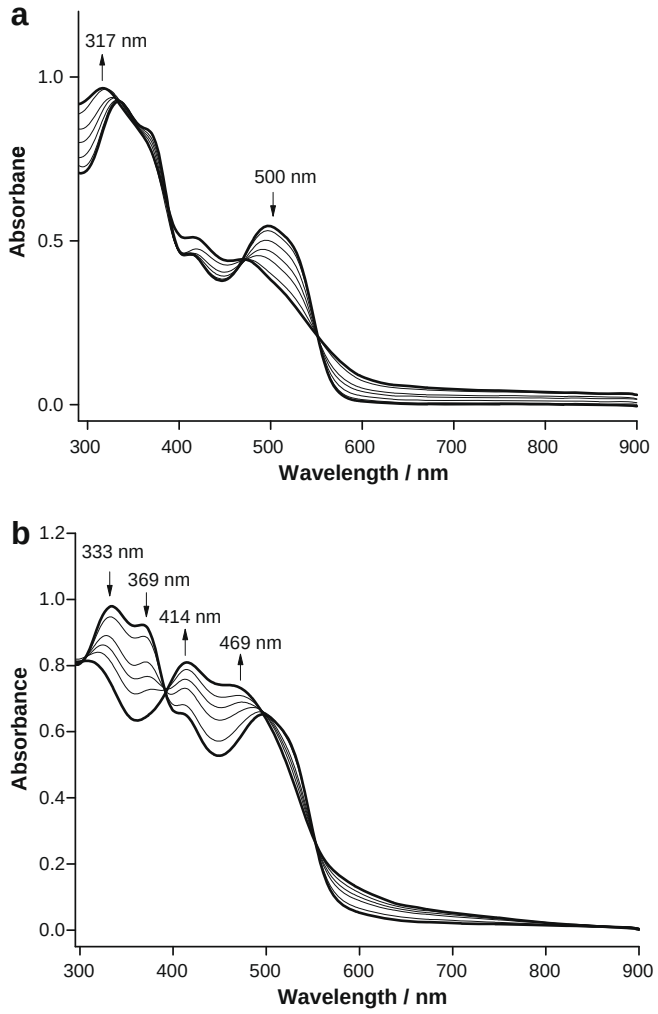

Fig. 9. Time-resolved UV–Vis spectra of $[\mathbf{Pd_2(L_2)_2}](\mathbf{Ac})_4$ in CH_2Cl_2 containing 0.4 M TBAP (a) during the oxidation at E_{app} = 1.35 V (b) during the reduction at E_{app} = −1.42 V.

on the ligand. The oxidation processes of $[\mathbf{Pd_2}(L_4)_2](\mathbf{Ac})_4$ is reversible with the corresponding anodic–cathodic peak separation (ΔE) (0.08 V at scan rate 0.010 V s^{-1}). The corresponding anodic wave (Ia) of the reduction process is not clear, but it is seen from the DPV (the inset figure) that the value of current during re-oxidation process (Ia) is one half relative to that of the reduction process (Ic), indicating a quasi-reversible reduction process. This result was also confirmed by spectroelectrochemical studies below.

The spectroelectrochemical behaviors of $[\mathbf{Pd_2}(L_4)_2](\mathbf{Ac})_4$ were investigated using a thin-layer UV–Vis spectroelectrochemical technique in CH_2Cl_2 solution containing 0.4 M TBAP. The UV–Vis spectral changes for the reduced and oxidized species were obtained in a thin-layer cell during applied potentials. The absorption spectra of electrochemically generated species are given in Fig. 9. The convenient values of applied potentials for *in situ* spectroelectrochemical experiment were determined for the reduction and oxidation processes by taking CVs of the metal complex in the thin-layer cell.

Fig. 9a shows the changes in the electronic spectra of $[\mathbf{Pd_2}(L_4)_2](\mathbf{Ac})_4$ during the oxidation process in the thin-layer cell. When the potential (E_{app} = 1.35 V) was applied in the thin-layer cell, the intensity of the main band at 500 nm belonging to the $n \rightarrow \pi^*$ transitions of the azomethine (CH=N) almost disappeared and the band at 335 nm shifted to a lower energy with a higher intensity. The well-defined isosbestic points were observed at 386, 470, and 550 nm, confirming that the electrode reaction proceeds in a quantitative fashion and therefore the absence of any coupled chemistry [2,3]. The original spectrum corresponding to the neutral complex could be recovered when the potential was applied at E_{app} = 0.50 V for the re-reduction process which indicates that the reduced species is stable and the process being reversible. Fig. 9b exhibits the changes in the electronic spectra of $[\mathbf{Pd_2}(L_4)_2](\mathbf{Ac})_4$ during the reduction process (the applied potential (E_{app}) = −1.42 V). As seen, the main bands at 500 shifted to 469 nm and the intensity of the band at 414 nm increased. Moreover, the intensity of the bands at 333 and 369 nm decreased. The well-defined isosbestic points were observed at 392 and 552 nm. The original spectrum of the neutral complex could be 70% recovered when the potential was applied at E_{app} = −0.50 V for the re-oxidation process, indicating that the single electro-reduced products remain almost stable in the thin-layer cell throughout the experiment and the process being quasi-reversible.

4. Conclusions

New sterically constrained Schiff-base ligands and their mono- and dinuclear Pd(II) complexes were synthesized and characterized by elemental analyses, FT-IR, UV–Vis, ^1H and ^{13}C NMR spectra, magnetic susceptibility measurements, molar conductivity and mass spectra. The mono- and dinuclear Pd(II) metal complexes were found to be active catalysts for the Suzuki–Miyaura cross-coupling of activated different aryl bromides with phenylboronic acid, using DMF as solvent. It can be seen that $[\mathbf{Pd_2}(L)_2](\mathbf{Ac})_4$ complexes are effective compounds for the coupling of aryl bromides with phenylboronic acid. We tested the reaction with deactivated aryl bromide such as 4-bromoanisole, but the coupling reaction did not occur under these conditions. So it has been that these complexes are uneffective complex for the deactivated aryl bromide. Also, catalytic studies showed that the mono- and dinuclear metal complexes (except for $[Pd(L_3)]$ complex at 45 °C) exhibited a catalytic activity toward the hydrogenation of nitrobenzene and cyclohexene under H_2 gas (760 Torr) in DMF solution at 25 and 45 °C.

Acknowledgements

This work was supported, in part, by the Technological and Scientific Research Council of Turkey TUBITAK (TBAG Project No: 106T085).

References

[1] R.H. Holm, M.J. O'Connor, Prog. Inorg. Chem. 14 (1971) 325.
[2] J. Vargas, J. Costamagna, R. Latorre, A. Alvardo, G. Mena, Coord. Chem. Rev. 119 (1992) 67.
[3] E. Tas, A. Kilic, N. Konak, I. Yilmaz, Polyhedron 27 (2008) 1024.
[4] A. Kilic, E. Tas, B. Deveci, I. Yilmaz, Polyhedron 26 (2007) 4009.
[5] (a) S. Yamada, Coord. Chem. Rev. 190 (1992) 537;
(b) D.E. Fenton, Chem. Soc. Rev. 28 (1999) 159.
[6] L. Canali, D.C. Sherrington, Chem. Soc. Rev. 28 (1999) 85.
[7] Y. Suzuki, H. Herao, T. Fujta, Bull. Chem. Soc. Jpn. 75 (2003) 1493.
[8] J. Stubbe, V.D. Donk, Chem. Rev. 98 (1998) 705.
[9] H.U. Blaser, B. Pugin, F. Spindler, J. Mol. Catal. A: Chem. 231 (2005) 1.
[10] H.U. Blaser, C. Malan, B. Pugin, F. Spindler, H. Steiner, M. Studer, Adv. Synth. Catal. 345 (2003) 103.
[11] M.J. Palmer, M. Wills, Tetrahedron Asymmetr. 10 (1999) 2045.
[12] S. Kannan, K.N. Kumar, R. Ramesh, Polyhedron 27 (2008) 701.
[13] A. Togni, L.M. Venanzi, Angew. Chem., Int. Ed. Engl. 33 (1994) 497.
[14] F. Fache, E. Schulz, M.L. Tommasino, M. Lemaire, Chem. Rev. 100 (2000) 2159.
[15] B. Clercq, F. Verpoort, Adv. Synth. Catal. 344 (2002) 639.
[16] O. Dayan, B. Cetinkaya, J. Mol. Catal. A: Chem. 271 (2007) 134.
[17] S. Burling, Adv. Synth. Catal. 347 (2005) 591.

[18] (a) A. Kilic, I. Yilmaz, M. Ulusoy, E. Tas, Appl. Organomet. Chem. 22 (2008) 494; (b) A. Kilic, F. Durap, M. Aydemir, A. Baysal, E. Tas, J. Organomet. Chem. 693 (2008) 2835.
[19] S.P. Stanforth, Tetrahedron 54 (1998) 263.
[20] J. Tsuji, Palladium Reagents and Catalysts: Innovations in Organic Synthesis, Wiley, Chichester, 1995.
[21] L. Botella, C. Najera, Angew. Chem., Int. Ed. 41 (2002) 1.
[22] A. Suzuki, J. Organomet. Chem. 576 (1999) 147.
[23] N. Miyaura, A. Suzuki, Chem. Rev. 95 (1995) 2457.
[24] S. Haber, H.J. Kleiner (Hoescht AG), DE 19527118: Chem. Abstr. 126 (1997) 185894.
[25] A. Earnshaw, Introduction to Magnetochemistry, Academic Press, London, 1968, p. 4.
[26] D.A. Alonso, C. Najera, C. Pacheco, Org. Lett. 2 (13) (2000) 1823.
[27] G. Schetty, E. Steiner, Helv. Chim. Acta 57 (1974) 2149.
[28] R.L. Lintvedt, K.A. Rupp, M.J. Heeg, Inorg. Chem. 27 (1988) 331.
[29] B. Crociani, M. Sala, A. Polo, G. Bombieri, Organometallics 5 (1986) 1369.
[30] V.T. Kasumov, E. Tas, F. Koksal, S. Ozalp-Yaman, Polyhedron 2 (24) (2005) 319.
[31] K.N. Kumar, R. Ramesh, Polyhedron 24 (2005) 1885.
[32] H. Temel, S. Ilhan, M. Aslanoglu, A. Kilic, E. Tas, J. Chin. Chem. Soc. 53 (2006) 1027.
[33] E. Tas, M. Aslanoglu, A. Kilic, O. Kaplan, H. Temel, J. Chem. Res. (S) 4 (2006) 242.
[34] M. Ulusoy, O. Sahin, O. Buyukgungor, B. Cetinkaya, J. Organomet. Chem. 693 (2008) 1895.
[35] L. Sacconi, M. Ciampolini, F. Maffio, F.P. Cavasino, J. Am. Chem. Soc. 84 (1962) 3245.
[36] R.L. Carlin, Transition Metal Chemistry, vol. 1, Marcel Dekker, New York, 1965.
[37] C. Fraser, B. Bosnich, Inorg. Chem. 33 (1994) 338.
[38] A.B.P. Lever, Inorganic Electronic Spectroscopy, Elsevier, Amsterdam, 1984.
[39] C. Ballie, J. Xiao, Tetrahedron 60 (2004) 4159.
[40] A.F. Littke, G.C. Fu, Angew. Chem., Int. Ed. 41 (2002) 4176.
[41] S. Demir, I. Ozdemir, B. Cetinkaya, Appl. Organomet. Chem. 20 (2006) 254.
[42] G. Altenhoff, R. Goddard, C.W. Lehmann, F. Glorius, J. Am. Chem. Soc. 126 (2004) 15195.